

Quantum Algorithm for Vibronic Dynamics: Case Study on Singlet Fission Solar Cell Design

Danial Motlagh,¹ Robert A. Lang,¹ Jorge A. Campos-Gonzalez-Angulo,^{2,3}
Tao Zeng,⁴ Alan Aspuru-Guzik,^{2,3,5,6} and Juan Miguel Arrazola¹

¹*Xanadu, Toronto, ON, M5G 2C8, Canada*

²*University of Toronto, Toronto, ON, M5S 3H6, Canada*

³*Vector Institute for Artificial Intelligence, Toronto, ON, M5G 1M1, Canada*

⁴*Department of Chemistry, York University, Toronto, ON, M3J 1P3, Canada*

⁵*Canadian Institute for Advanced Research (CIFAR), Toronto, ON, M5G 1M1, Canada*

⁶*Acceleration Consortium, Toronto, ON, M5S 3H6, Canada*

Vibronic interactions between nuclear motion and electronic states are critical for the accurate modeling of photochemistry. However, accurate simulations of fully quantum non-adiabatic dynamics are often prohibitively expensive for classical methods beyond small systems. In this work, we present a quantum algorithm based on product formulas for simulating time evolution under a general vibronic Hamiltonian in real space, capable of handling an arbitrary number of electronic states and vibrational modes. We develop the first trotterization scheme for vibronic Hamiltonians beyond two electronic states and introduce an array of optimization techniques for the exponentiation of each fragment in the product formula, resulting in a remarkably low cost of implementation. To demonstrate practical relevance, we outline a proof-of-principle integration of our algorithm into a materials discovery pipeline for designing more efficient singlet fission-based organic solar cells. Based on commutator bounds, we estimate that a 100 femtosecond evolution using a second-order Trotter product formula of a 4-state model of an anthracene-fullerene interface requires 117 qubits and 1.5×10^7 Toffoli gates in a reduced dimensionality of 11 modes. In its full dimensionality of 246 modes, it requires 1065 qubits and 2.7×10^9 Toffoli gates.

I. INTRODUCTION

Much of the effort in applying quantum computers to problems in quantum chemistry has been concerned with electronic structure, particularly with the computation of ground state energies of the electronic Hamiltonian [1]. While of great importance, electronic structure on its own is not a complete description of molecular behavior, as it neglects the crucial role of vibronic effects caused by nuclear vibrational motions interacting with electronic states. Furthermore, it remains unclear whether electronic structure is where quantum advantage will be found [2]. Accurate vibronic simulations are essential for understanding photo-induced processes, such as non-radiative relaxation and energy transfer, and are instrumental in interpreting experimental spectra [3, 4]. Studying such processes has many applications across a wide range of technologies. These include designing advanced materials for optoelectronic and photovoltaic technologies [5, 6], studying molecular photomagnets for ultradense memory storage [7–11], enhancing the performance of thermally activated delayed fluorescence (TADF)-based organic light-emitting diodes (OLEDs) [12–15], discovering improved sunscreens [16–19], and advancing photodynamic therapies for cancer treatment [20–23]. Moreover, vibronic effects shed light on photo-excited biological processes, such as those in biological light-harvesting complexes [24, 25] and DNA [26–28]. However, despite their importance, full non-adiabatic dynamics are too resource-intensive for classical methods and are often omitted in materials discovery pipelines.

Many excited-state scenarios encountered in photochemistry, such as conical intersections and avoided crossings, require a description beyond the Born-Oppenheimer approximation [29–31]. There has been much effort in developing numerical methods for performing non-adiabatic dynamics. Semi-classical methods, like trajectory surface hopping [32–35] and Ehrenfest dynamics [36–40] can be efficient but fail to capture important quantum phenomena such as coherence, tunneling, and wavepacket branching. For molecular applications, the most ubiquitously employed method for propagation according to the time-dependent Schrödinger equation is the multi-configurational time-dependent Hartree (MCTDH) method [31, 41, 42], along with related techniques [43–46]. However, these methods are approximate, their use requires high levels of expertise, and have unfavorable scaling with increased accuracy, limiting them to small systems and short propagation times [47, 48]. Quantum computers offer an alternative to overcoming these limitations [49–51]; however, little attention has been given to this topic in quantum computing. Analog quantum simulators have gathered particular interest, but they currently face scalability issues for large-scale calculations [52, 53]. Alternative digital-based algorithms have been explored [54], but these results are limited in scope and not applicable to general vibronic Hamiltonians with an arbitrary number of diabatic states or arbitrary forms of mode interactions.

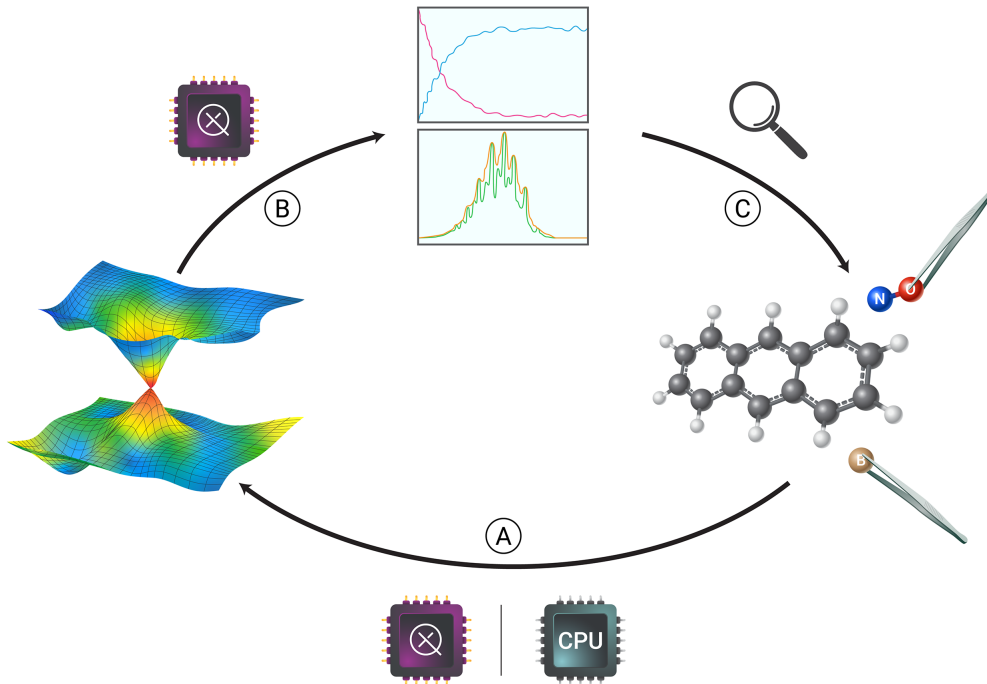


FIG. 1. Proof-of-principle integration of our quantum algorithm into a materials discovery workflow. (A) Following the initialization or modification of a molecule, electronic structure calculations are performed, leveraging either quantum or classical resources to construct the vibronic model. For vibronic Hamiltonians employed in ultrafast photochemistry, this procedure typically includes geometry optimization, a normal-mode analysis following the calculation of the Hessian, and excited-state calculations at points along normal mode displacements. (B) The non-adiabatic dynamics for the vibronic Hamiltonian are performed on a quantum computer using the algorithm presented in Section III, producing observable quantities such as diabatic state populations and photoabsorption spectra. (C) The interpretation of the output observables is used to inform a change to molecular candidates to optimize properties such as transition rates and excited-state lifetimes.

In this work, we develop a quantum algorithm based on product formulas for time evolution under a general vibronic Hamiltonian with an arbitrary number of states and modes. One of the main technical novelties of our algorithm is a trotterization scheme for vibronic Hamiltonians beyond two electronic states. We also develop an array of optimization techniques deployed in the exponentiation of each fragment in the product formula to significantly reduce the cost of its implementation. After introducing the algorithm, we analyze its complexity and address initial state preparation relevant to photochemistry, showing that it incurs negligible cost compared to the simulation. Finally, we discuss the efficient extraction of observables specific to vibronic dynamics on a quantum computer. In particular, we show that extracting electronic state populations—the key observable in vibronic simulation—only requires measuring the few-qubit electronic register in the computational basis. This contrasts with typical energy-based observables requiring controlled implementations of the time evolution operator. Combined with cheap initial state preparation, this solves the input-output problem often faced in other applications of quantum computing.

Next, we discuss applications of our algorithm, with a particular focus on its relevance for organic solar cells based on the physical process of singlet fission (SF) [55–57], a form of multiple exciton generation that allows the production of two excitons from just one photon. This makes SF-based solar cells potentially capable of producing two pairs of free charge carriers from each photon, enhancing the overall efficiency. To date, only a handful of SF chromophores have been discovered. This scarcity is commonly recognized as the most significant barrier to realizing SF-based solar cells [58–62]. We outline our vision for how the quantum algorithm can be utilized to accelerate the discovery of SF chromophores by elucidating how dynamical processes, such as singlet fission, triplet separation, and charge transfer rates, can be probed and optimized for using our algorithm. Lastly, we provide resource estimates for relevant systems of interest in Table I, showing, using commutator bounds, that a 100 femtosecond evolution of a 4-state, 246-mode model of an anthracene-fullerene interface [63] requires 1065 qubits and 2.7×10^9 Toffoli gates. It is worth noting that estimates based on commutator bounds tend to pessimistically overestimate runtime. Hence, actual runtimes will likely be even smaller.

The manuscript is structured as follows. In Section II, we briefly review the construction of the vibronic Hamiltonian. We then introduce the quantum algorithm for performing vibronic dynamics, initial state preparation, and extracting observables in Section III. In Section IV, we outline a proof-of-principle workflow where scalable quantum simulation of non-adiabatic dynamics could provide utility in the context of singlet fission-based solar cell materials discovery.

II. BACKGROUND

Vibronic interactions become important whenever electronic states are energetically degenerate or pseudo-degenerate. In the adiabatic basis, the eigenstates of the electronic Hamiltonian interact with one another through non-adiabatic couplings, which can give rise to singularities. A practical workaround for this problem is propagating the molecular time-dependent Schrödinger equation using a diabatic electronic basis, in which the couplings are potential terms varying smoothly with nuclear coordinates. For many photochemical scenarios, it is standard procedure to employ the Köppel-Domcke-Cederbaum (KDC) vibronic Hamiltonian [64],

$$H = \mathbb{I}_{\text{el}} \otimes (T_{\text{nuc}} + V_0) + \mathbf{W}. \quad (1)$$

Here, T_{nuc} and V_0 are, respectively, the vibrational kinetic and potential energy operators obtained from the harmonic approximation to the electronic ground state's potential energy surface [31]

$$T_{\text{nuc}} = \frac{1}{2} \sum_r \omega_r P_r^2, \quad V_0 = \frac{1}{2} \sum_r \omega_r Q_r^2, \quad (2)$$

where $P_r = -i\partial/\partial Q_r$ and ω_r are, respectively, the momentum operator and the harmonic frequency associated with mode r . The diabatic potential $\mathbf{W} = \mathbf{W}^{(0)} + \mathbf{W}^{(1)}(\vec{Q}) + \mathbf{W}^{(2)}(\vec{Q}) + \dots$, is Taylor expanded at a reference nuclear geometry, typically that at equilibrium, in a set of dimensionless normal vibrational mode coordinates \vec{Q} . To account for spin-forbidden transitions, such as intersystem crossing, \mathbf{W} may be augmented with the inclusion of spin-orbit coupling terms $\mathbf{W}' = \mathbf{W} + \mathbf{H}_{SO}$, making \hat{H} a spin-vibronic Hamiltonian [65–67]. Given N (spin-)diabatic electronic states (“diabats”), \mathbf{W}' is an $N \times N$ block matrix where each block is of the general form

$$\mathbf{W}'_{ij}(\vec{Q}) = \lambda^{(i,j)} + \sum_r a_r^{(i,j)} Q_r + \sum_{rr'} b_{rr'}^{(i,j)} Q_r Q_{r'} + \dots, \quad (3)$$

The parameters $\lambda^{(i,j)}$, $a_r^{(i,j)}$, $b_{rr'}^{(i,j)}$, \dots are coupling constants describing the interaction between the i th and j th diabats induced by the modes labeled by r , r' , etc. These values can be obtained from electronic structure calculations and diabaticization protocols, for which various approaches exist [24, 66, 68–76]. In the presence of spin-orbit coupling, the coupling constants may become complex.

The accuracy and complexity of the (spin-)vibronic Hamiltonian is determined by the diabatic states and vibrational modes included, the expansion order of \mathbf{W}' , and the determined coupling constants. Typically, the matrix elements of Eq. (3) are truncated to first order, yielding the linear vibronic coupling (LVC) model [64]. Truncation to quadratic vibronic coupling (QVC) is also common, depending on the problem [77]. The LVC and QVC models often capture qualitative vibronic interactions and suffice for small amplitude distortions [78]. However, higher-order expansions are needed for quantitative spectra and dynamics involving longer timescales, large amplitude motions, or highly anharmonic potentials [31, 79–85].

We utilize a discretization over a grid to implement the operators Q and P in a real-space representation. Ref. [86] provides a detailed derivation of the procedure along with a comprehensive investigation of the discretization error. In particular, they show that the discretization error decreases exponentially with the number of grid points. We will make use of the same discretization protocol. Working in real space with $K = 2^k$ grid points, we take the eigenvectors of Q to be the k -qubit computational basis states with eigenvalues

$$Q|x\rangle = \Delta(x - K/2)|x\rangle, \quad (4)$$

for integer $x \in \{0, 1, \dots, K-1\}$ and $\Delta = \sqrt{2\pi/K}$. The momentum operator P is related to Q via the quantum Fourier transform (QFT) as

$$P = \text{QFT}^\dagger \cdot X_{k-1} \cdot Q \cdot X_{k-1} \cdot \text{QFT}, \quad (5)$$

where X_{k-1} is an X gate on the most significant qubit.

III. QUANTUM ALGORITHM

This section describes our algorithm for time evolution under a vibronic Hamiltonian. One key technical contribution is providing the first trotterization scheme for vibronic Hamiltonians extending beyond two electronic states. This is done using the partitioning in Eq. (7) and the corresponding technique to block-diagonalize each fragment of the Hamiltonian. Our next key contribution is the heavily-optimized implementation of time evolution for each fragment after block-diagonalization. Namely, we can reduce the cost of exponentiating the block-diagonal matrix in Eq. (10) to essentially have the same cost as the exponentiation of a single block. Lastly, we provide further optimization via a caching protocol described in Section III A that strategically stores parts of the calculation to avoid redundant computations later.

Given $N = 2^n$ electronic states and M vibrational modes, with each mode discretized into $K = 2^k$ points, the vibronic Hamiltonian acting on the space of $M \log(N) \log(K)$ qubits can be written as $H = T + V$ for

$$T = \mathbb{I}_{\text{el}} \otimes \sum_{r=0}^{M-1} \frac{\omega_r}{2} P_r^2, \quad V = (\mathbb{I} \otimes V_0) + \mathbf{W}' = \sum_{i,j=0}^{N-1} |j\rangle \langle i| \otimes V_{ji}, \quad (6)$$

where each $V_{ji} = \sum_{|\vec{\alpha}| \leq d} c_{\vec{\alpha}}^{(j,i)} \mathbf{Q}^{\vec{\alpha}} = \lambda^{(j,i)} + \sum_{r=0}^{M-1} \gamma_r^{(j,i)} Q_r + \sum_{r,r'=0}^{M-1} \beta_{rr'}^{(j,i)} Q_r Q_{r'} + \dots$ is a d -degree multivariate polynomial of position operators. Here, we have used the multi-index notation $\mathbf{Q}^{\vec{\alpha}} = Q_0^{\alpha_0} Q_1^{\alpha_1} \dots Q_{M-1}^{\alpha_{M-1}}$. As shown later, position and momentum operators in the real-space representation can be exponentiated cheaply on a quantum computer, making the implementation of operators like $e^{itV_{ij}}$ and e^{itT} straightforward. This motivates the use of Trotter product formulas for implementing e^{itH} ; however, to do this, we need first to decompose $H = \sum_m H_m$ such that each e^{itH_m} can be implemented in a fast forwardable manner. We do this by writing $V = \sum_{m=0}^{N-1} H_m$ for

$$H_m = \sum_{j=0}^{N-1} |j\rangle \langle m \oplus j| \otimes V_{j,m \oplus j}, \quad (7)$$

where $m \oplus j = \sum_{s=0}^{n-1} (\tilde{m}_s \oplus \tilde{j}_s) \cdot 2^s$ is the integer resulting from the bitwise XOR product between the bitstring representations of integers $m = \sum_{s=0}^{n-1} \tilde{m}_s \cdot 2^s$ and $j = \sum_{s=0}^{n-1} \tilde{j}_s \cdot 2^s$. Notice that the block-diagonal fragment $e^{itH_0} = e^{it \sum_j |j\rangle \langle j| \otimes V_{jj}} = \sum_j |j\rangle \langle j| \otimes e^{itV_{jj}}$ reduces to a sequence of evolutions $e^{itV_{jj}}$ controlled by the corresponding electronic state $|j\rangle$. Our strategy then becomes clear: block-diagonalize each e^{itH_m} and implement them like e^{itH_0} . For simplicity, in what follows, we assume the coefficients in V_{ji} are real, implying $V_{ji} = V_{ij}$. This assumption is not essential as the algorithm described below can be adapted to the case where $V_{ji} = V_{ij}^\dagger$ by separating the Hermitian and anti-Hermitian parts of V_{ji} .

If \tilde{m} has Hamming weight 1, that is j and $m \oplus j$'s bitstring representations only differ in a single bit, we can block-diagonalize H_m by applying a Hadamard on both sides of the qubit where they differ since $(\text{Had})X(\text{Had}) = Z$. To see this, without loss of generality, assume the rightmost qubit is the differing one; then, we have

$$(\text{Had})H_m(\text{Had}) = \sum_{j'=0}^{N/2-1} |j'\rangle \langle j'| \otimes (\text{Had})X(\text{Had}) \otimes V_{(2j'),(2j'+1)} = \sum_{j'=0}^{N/2-1} |j'\rangle \langle j'| \otimes Z \otimes V_{(2j'),(2j'+1)}. \quad (8)$$

If \tilde{m} has Hamming weight greater than 1, we construct a unitary U by choosing one of the qubits where \tilde{m} is 1 and using it as a control to apply a CNOT to all other qubits where \tilde{m} is 1. This ensures that the pairs $U|j\rangle \langle m \oplus j| U^\dagger$ only differ in a single qubit, the qubit used as the control. To see this, notice how a CNOT gate fixes one of the mismatches between two pairs differing in both bits:

$$\text{CNOT} |b_2 b_1\rangle \langle \bar{b}_2 \bar{b}_1| \text{CNOT} = |b_1 \oplus b_2, b_1\rangle \langle \bar{b}_1 \oplus \bar{b}_2, \bar{b}_1| = |b_1 \oplus b_2, b_1\rangle \langle b_1 \oplus b_2, \bar{b}_1|, \quad (9)$$

where we've used $b_1 \oplus b_2 = \bar{b}_1 \oplus \bar{b}_2$. Hence, $UH_m U^\dagger$ can be block-diagonalized by applying a Hadamard on the control qubit. We have shown how to block-diagonalize each fragment e^{itH_m} to be implemented in the same manner as e^{itH_0} , now we give our algorithm for the implementation of e^{itH_0} . For simplicity, we absorb t into H_0 for the rest of the discussion.

A naive implementation of $e^{iH_0} = e^{i \sum_j |j\rangle \langle j| \otimes V_{jj}} = \sum_j |j\rangle \langle j| \otimes e^{iV_{jj}}$ would be to perform the corresponding evolution $e^{iV_{jj}}$ on the vibrational space controlled by the corresponding state $|j\rangle$ for all N electronic states. This would have a

cost of N times that of a single controlled evolution $e^{iV_{jj}}$. Our next key result is an algorithm to implement e^{iH_0} with essentially the same cost as implementing a single uncontrolled evolution $e^{iV_{jj}}$. From Eq. (4), we have that $Q|x\rangle = \Delta(x - 2^{k-1})|x\rangle$. However, if we interpret the computational basis state bitstrings in the signed integer representation, we will have $Q|x\rangle = \Delta \cdot x|x\rangle$. Accordingly, all the arithmetic operations below will correspond to signed arithmetic. Using this framework, we can write the action of e^{iH_0} on any computational basis state $|j\rangle|\mathbf{x}\rangle = |j\rangle \otimes_{r=0}^{M-1} |x_r\rangle$ as

$$\begin{aligned} \sum_j |j\rangle \langle j| \otimes e^{iV_{jj}} &= \sum_{j,\mathbf{x}} |j\rangle \langle j| \otimes |\mathbf{x}\rangle \langle \mathbf{x}| \cdot \exp \left(i \sum_{|\bar{\alpha}| \leq d} \Delta^{|\bar{\alpha}|} \cdot c_{\bar{\alpha}}^{(j,j)} \mathbf{x}^{\bar{\alpha}} \right) \\ &= \prod_{|\bar{\alpha}| \leq d} \sum_{j,\mathbf{x}} |j\rangle \langle j| \otimes |\mathbf{x}\rangle \langle \mathbf{x}| e^{i\Delta^{|\bar{\alpha}|} \cdot c_{\bar{\alpha}}^{(j,j)} \mathbf{x}^{\bar{\alpha}}}. \end{aligned} \quad (10)$$

Therefore, we can implement $e^{iH_0} = \sum_j |j\rangle \langle j| \otimes e^{iV_{jj}}$ by implementing each $\sum_{j,\mathbf{x}} |j\rangle \langle j| \otimes |\mathbf{x}\rangle \langle \mathbf{x}| \cdot \exp \left(i\Delta^{|\bar{\alpha}|} \cdot c_{\bar{\alpha}}^{(j,j)} \mathbf{x}^{\bar{\alpha}} \right)$ in Eq. (10). To implement each $\sum_{j,\mathbf{x}} |j\rangle \langle j| \otimes |\mathbf{x}\rangle \langle \mathbf{x}| \cdot \exp \left(i\Delta^{|\bar{\alpha}|} \cdot c_{\bar{\alpha}}^{(j,j)} \mathbf{x}^{\bar{\alpha}} \right)$ we

1. Load the binary representation of the coefficients $c_{\bar{\alpha}}^{(j,j)}$ in an ancillary register controlled on the corresponding electronic state using a series of multi-controlled multi- X gates.
2. Compute the corresponding variable $\mathbf{x}^{\bar{\alpha}}$ in another register using signed quantum arithmetic by taking the product between the corresponding mode registers.
3. Compute the product between the coefficient and the variable $c_{\bar{\alpha}}^{(j,j)} \mathbf{x}^{\bar{\alpha}}$.
4. Perform a phase gradient operation with scaling factor $\Delta^{|\bar{\alpha}|}$ on the register holding the value $c_{\bar{\alpha}}^{(j,j)} \mathbf{x}^{\bar{\alpha}}$.
5. Uncompute all intermediate results.

Here a b -qubit phase gradient operation with scaling factor δ is defined as $\text{PhaseGrad}(\delta) = \sum_{y=0}^{2^b-1} e^{i\delta y/2^b} |y\rangle \langle y|$. To give a concrete example, the sequence of operations for implementing $\sum_j |j\rangle \langle j| \otimes \exp \left(i c_{(1,1)}^{(j,j)} Q_0 Q_1 \right)$ for a 2-mode system would be

$$\begin{aligned} |j\rangle |0\rangle |0\rangle |0\rangle |x_1\rangle |x_0\rangle &\xrightarrow{\text{Ctrl-Load}} |j\rangle |0\rangle |c_{(1,1)}^{(j,j)}\rangle |0\rangle |x_1\rangle |x_0\rangle \\ &\xrightarrow{\text{Q-Arithmetic}} |j\rangle |0\rangle |c_{(1,1)}^{(j,j)}\rangle |x_0 x_1\rangle |x_1\rangle |x_0\rangle \\ &\xrightarrow{\text{Q-Arithmetic}} |j\rangle |c_{(1,1)}^{(j,j)} x_0 x_1\rangle |c_{(1,1)}^{(j,j)}\rangle |x_0 x_1\rangle |x_1\rangle |x_0\rangle \\ &\xrightarrow{\text{PhaseGrad}(\Delta^2)} \exp \left(i\Delta^2 \cdot c_{(1,1)}^{(j,j)} x_0 x_1 \right) |j\rangle |c_{(1,1)}^{(j,j)} x_0 x_1\rangle |c_{(1,1)}^{(j,j)}\rangle |x_0 x_1\rangle |x_1\rangle |x_0\rangle \\ &\xrightarrow{\text{Uncompute}} \exp \left(i\Delta^2 \cdot c_{(1,1)}^{(j,j)} x_0 x_1 \right) |j\rangle |0\rangle |0\rangle |0\rangle |x_1\rangle |x_0\rangle. \end{aligned} \quad (11)$$

The advantage of implementing $\sum_j |j\rangle \langle j| \otimes e^{iV_{jj}}$ this way is that we only need to control the value of the coefficients that are loaded based on the state of the electronic register $|j\rangle$ to control the evolutions $e^{iV_{jj}}$ on the state of the electronic register.

Lastly, we show the implementation of e^{iT} . The operator e^{iT} reduces to $\exp \left(\frac{i}{2} \sum_{r=0}^{M-1} \omega_r P_r^2 \right)$ on the vibrational space. It can be implemented by applying $\exp \left(\frac{i}{2} \omega_r P_r^2 \right)$ to each corresponding mode, where P_r is the momentum operator of the r^{th} mode related to Q_r by Eq. (5). Hence, after diagonalizing via QFT, $\exp \left(\frac{i}{2} \omega_r P_r^2 \right)$ can be implemented in a similar manner as $\exp \left(\frac{i}{2} \omega_r Q_r^2 \right)$. Writing $H_N = T$ for completeness, we can have $H = \sum_{m=0}^N H_m$. Hence, we can implement e^{itH} using a Trotter product formula. The first-order formula $U_1(\theta)$ and second-order formulas $U_2(\theta)$ will have the form

$$U_1(\theta) = \prod_{m=0}^N e^{i\theta H_m} = e^{i\theta H} + \mathcal{O}(\theta^2), \quad (12)$$

$$U_2(\theta) = \prod_{m=0}^N e^{i\theta H_m} \prod_{m=N}^0 e^{i\theta H_m} = e^{i\theta H} + \mathcal{O}(\theta^3). \quad (13)$$

A. Optimization via Caching

In this section, we provide a further optimization of the algorithm based on a caching protocol. The motivation behind this approach is to avoid redundant calculations when implementing higher-degree terms in the polynomial. Consider the implementation of a term like $\exp(i\theta Q_s Q_t Q_r)$ in our algorithm. This requires computing the product of the corresponding modes $|x_s x_t x_r\rangle$ which involves first calculating $|x_s x_t\rangle$ and then multiplying the result with $|x_r\rangle$ to obtain $|x_s x_t x_r\rangle$. However, we have already computed the intermediate product $|x_s x_t\rangle$ when implementing the term $\exp(i\theta' Q_s Q_t)$. Instead of uncomputing this intermediate result after its use, we can cache it for reuse. By retaining $|x_s x_t\rangle$, we can compute $|x_s x_t x_r\rangle$ by a single multiplication with $|x_r\rangle$, thereby saving an additional computation and uncomputation of $|x_s x_t\rangle$. In fact, we can do this for every $r = 0, \dots, M-1$. More generally, we can extend this idea to terms of arbitrary degree. Terms of degree L can reuse computations from terms of degree $L-1$, which in turn reuse computations from terms of degree $L-2$, and so on.

For the most space-efficient implementation of this caching protocol, we utilize a *depth-first search* approach in determining the order in which we exponentiate the terms in the polynomial. We organize the computation of terms in a tree-like structure where each node represents a term, and edges represent the dependency of higher-degree terms on lower-degree ones. Then, the order of implementation is given by a depth-first search traversal of this tree starting from terms of degree 1. This ensures that every term of degree $L > 1$ reuses the computation from a term of degree $L-1$ in a way that, at any given time, we are only caching one term at each degree.

B. Complexity Analysis

Here, we present the runtime and space complexity of our algorithms for implementing a single Trotter step in Eq. (12). The proof and a more detailed analysis are provided in Appendix A.

Theorem 1. *Let N be the number of electronic states, M be the number of vibrational modes, and K be the number of grid points per mode. Define the vibronic Hamiltonian as $H = \mathbb{I}_{el} \otimes \sum_{r=0}^{M-1} \frac{\omega_r}{2} P_r^2 + \sum_{j,i=0}^{N-1} |j\rangle \langle i| \otimes V_{ji}$, where each $V_{ji} = \sum_{|\vec{\alpha}| \leq d} c_{\vec{\alpha}}^{(j,i)} \mathbf{Q}^{\vec{\alpha}}$ is a d -degree multivariate polynomial of position operators. Let H_m be defined as in Eq. (7) for $0 \leq m < N$ and let $H_N = \mathbb{I}_{el} \otimes \sum_{r=0}^{M-1} \frac{\omega_r}{2} P_r^2$ so $H = \sum_{m=0}^N H_m$. Then for $\epsilon, \theta \in [0, 1]$ we can implement*

$$\prod_{m=0}^N e^{i\theta H_m + \mathcal{O}(\epsilon)},$$

using $\mathcal{O}(NM^d [d \log(K)^2 + \log(M^d/\epsilon)] + N^2 \log(N))$ T gates and $\mathcal{O}(d^2 \log(MK) + d \log(1/\epsilon) + N)$ ancilla qubits.

Notice that the complexity of our algorithm is highly dependent on the degree of the expansion in V_{ji} since a d -degree multivariate polynomial over M modes will generally have $\mathcal{O}(M^d)$ terms. In practice, d is small, often around 2 to 4, and higher degree terms are sparse, usually restricted to terms involving no more than 2 different modes at a time (e.g., $Q_r^2 Q_{r'}$).

C. Initial State Preparation

Preparing physically relevant initial states is crucial in extracting useful information from simulations. For photo-induced dynamics, the initial state often corresponds to a vertical excitation of the system, which has a simple product form

$$|\psi(0)\rangle = |j\rangle_{el} \bigotimes_{r=0}^{M-1} |\chi_0\rangle, \quad (14)$$

where $|j\rangle_{el}$ is the corresponding excited electronic state (represented as a computational basis in our model), and $|\chi_0\rangle$ is the harmonic oscillator ground state. State $|\chi_0\rangle$ corresponds to the discretized Hermite-Gauss function of zeroth order. If each mode is discretized into $K = 2^k$ grid points, $|\chi_0\rangle$ is then the k -qubit state

$$|\chi_0\rangle = \frac{1}{Z} \sum_{x=0}^{K-1} \exp\left(\frac{-\pi \cdot (x - \frac{K}{2})^2}{K}\right) |x\rangle, \quad (15)$$

where Z is the normalization constant such that $\|\chi_0\rangle\| = 1$. Methods to prepare Gaussian states are discussed in Refs. [87–89]. Instead of starting in a specific electronic state, we can choose to start in a superposition of electronic states. This choice is especially relevant for absorption/emission spectroscopy, where the initial state of the electronic register is the superposition resulting from the electronic ground state being acted upon by the dipole operator μ :

$$|\psi(0)\rangle = \frac{\mu|0\rangle_{\text{el}}}{\|\mu|0\rangle\|} \bigotimes_{r=0}^{M-1} |\chi_0\rangle = \left(\sum_{j=0}^{N-1} \mu_{j,0} |j\rangle \right) \bigotimes_{r=0}^{M-1} |\chi_0\rangle, \quad (16)$$

where $\mu_{j,0} = \frac{\langle j|\mu|0\rangle}{\|\mu|0\rangle\|}$. $\sum_{j=0}^{N-1} \mu_{j,0} |j\rangle$ is a state of small dimensionality that can be prepared using any black-box state preparation algorithm [90–92]. The product form of the states in Eq. (14) and Eq. (16) together with the fact that the size of each register will be small in practice, the cost of state preparation will be negligible compared to the cost of the simulation.

D. Observables

Following the development and analysis of our algorithm, the next critical step is identifying relevant observables for extracting meaningful information from simulations. Key observables of interest in vibronic simulations include electronic state populations and spectroscopic quantities.

1. Electronic State Populations

In the context of vibronic simulations, electronic state populations describe the probability of finding the system in a particular diabatic electronic state at a given time. For $|\psi(t)\rangle = e^{iHt} |\psi(0)\rangle$, the population of diabatic state $|j\rangle$ at time t is given by

$$p_j(t) = \langle \psi(t) | (|j\rangle \langle j| \otimes \mathbb{I}_{\text{vib}}) | \psi(t) \rangle. \quad (17)$$

In our model, estimating Eq.(17) simply corresponds to measuring the electronic register in the computational basis and collecting statistics. This allows us to simultaneously estimate populations of all states using $\mathcal{O}(\epsilon^{-2})$ measurements for an ϵ accurate estimation. Alternatively, to estimate the population of any particular state, the quantum amplitude estimation (QAE) algorithm [93] can be employed, which, at the cost of a longer circuit depth, reduces the total runtime to $\mathcal{O}(\epsilon^{-1})$.

The state populations obtained throughout propagation can then be straightforwardly fitted to exponential functions or applied within more sophisticated kinetic models to extract transition rates and excited-state lifetimes [47]. This ability enables the study of key physical phenomena such as non-radiative relaxation via intersystem crossing and internal conversion, as well as exciton transfer and charge transfer. Studying these phenomena is crucial for uncovering reaction pathways in photochemistry, as well as designing materials for optoelectronic and photovoltaic technologies.

2. Spectroscopic Quantities

Spectroscopic quantities are another class of fundamental observables in vibronic simulations. Specifically, absorption and emission spectra are readily obtained via a Fourier transform of the dipole autocorrelation function

$$C(\omega) = \frac{1}{2\pi} \int_{-\infty}^{\infty} dt e^{-i\omega t} \langle \psi | e^{iHt} \mu e^{-iHt} \mu | \psi \rangle, \quad (18)$$

which provide insights into the interaction of molecules with electromagnetic radiation. Here, μ is the dipole moment operator, and $|\psi\rangle$ is the reference state, often taken to be the state from Eq. (16).

The recently developed framework of generalized quantum phase estimation and related techniques [94, 95] enable the efficient extraction of linear and non-linear spectroscopic quantities on a quantum computer. In particular, the technique of generalized quantum phase estimation [94] allows one to directly sample from the absorption spectra of a system with an energy resolution η when given access to the time evolution of the system for $t \sim \mathcal{O}(1/\eta)$. The absorption and emission spectra are essential for understanding and predicting optical properties such as brightness, color purity, and stability in materials; this can guide the design of new materials for optoelectronic devices like organic lasers and light-emitting diodes (OLEDs).

IV. APPLICATIONS IN SINGLET FISSION SOLAR CELL DESIGN

This section discusses how our quantum algorithm from Section III could be integrated into a materials discovery pipeline in an industrial setting. While simulations of excited-state dynamics have extensive industrial applications ranging from optoelectronic technologies to non-invasive cancer therapies[96], here we focus on the specific case of singlet fission (SF) solar cells and how our algorithm can be utilized to accelerate the discovery of candidate SF chromophores.

As global energy demands rise, the reliance on unsustainable energy sources poses significant environmental and economic challenges. Solar energy offers a scalable and sustainable solution; however, conventional photovoltaics are restricted by the Shockley-Queisser limit [97], which puts an upper bound of $\sim 33\%$ on the power conversion efficiency that a single junction solar cell can have. Consequently, significant efforts have been put towards going beyond this limit with *singlet fission* (SF) [98], a type of multi-exciton generation process, emerging as a promising direction. SF-based solar cells can, in principle, achieve a theoretical internal quantum efficiency of 200%: two electrons for one photon [58, 99–101]. However, commercialization of SF solar cells has been hindered by the fact that only a handful of candidate SF chromophores have been discovered to date. This scarcity is commonly recognized as the most significant barrier preventing the realization of SF technologies [58–62].

To overcome this challenge, computational search via *ab initio* simulations has been proposed as a promising route to accelerating the discovery of viable SF-based solar cell materials [100]. Energetic criteria can serve as a good initial screening tool as they provide insight into whether the process of SF is energetically allowed. However, the rate of SF is of greater importance to the success of an SF chromophore, as the process must outcompete other relaxation paths operating on ultrafast timescales. Despite this, proposals so far for the computational design and screening of new SF chromophores have almost entirely relied on assessment based on static electronic energy criteria [59, 102–104]. However, considering only electronic excitation energies is far from being enough. This is because SF is an excited-state dynamical process in which vibronic interaction is of central importance and should not be ignored. [56, 58, 100, 105–116]. Semi-classical methods such as surface hopping fail to capture important quantum effects involved in SF, such as tunneling [117, 118]. On the other hand, tackling the fully quantum simulation via methods like MCTDH beyond a model with reduced dimensionality quickly becomes too resource-intensive, or intractable altogether, for integration into a computational discovery pipeline. A highly optimized and scalable quantum algorithm like the one provided in Section III lifts the above bottleneck and allows for a more effective computational search of new SF chromophores.

A. Overview

To provide a concrete example of how our quantum algorithm for non-adiabatic dynamics could enable the discovery of new SF materials for solar cells, a high-level discovery workflow is illustrated in Fig. 1. Starting with an initial candidate molecule, a vibronic model Hamiltonian is constructed from electronic structure calculations, utilizing either classical or quantum resources. Once the vibronic Hamiltonian has been constructed, our algorithm performs the subsequent non-adiabatic dynamics simulations from where it extracts relevant observables such as state populations or absorption spectra as described in Section III D. This dynamical information is then used to guide modifications (e.g., functional group or heteroatom substitutions [62, 119, 120]) to the candidate molecule, either through expert interpretation or machine learning approaches such as Bayesian optimization [121–123]. This process could be iterated to optimize for properties of interest or generate high-quality data for complimentary computer-aided design workflows. Furthermore, the ability to rapidly perform non-adiabatic simulations following the modification of a molecular system can provide indispensable mechanistic insights into properties of interest. For instance, changes to the state population dynamics following molecular modification would offer valuable information on the complicated interplay between molecular geometry, electronic structure, and dynamical pathways, from which revised rational design principles could be proposed [124–126].

In the following subsection, we describe a more detailed proof-of-principle pipeline for the design of new SF chromophores as illustrated in Fig. 2 by applying the workflow of Fig. 1 to the various vibronically driven processes crucial in determining the efficiency of SF solar cells. We briefly introduce each process, their modeling on a quantum computer, and the corresponding restricted space over which the computational search could be performed. Furthermore, we report estimated runtimes on a quantum computer, for example, systems in Table I to demonstrate the efficiency of our quantum algorithm.

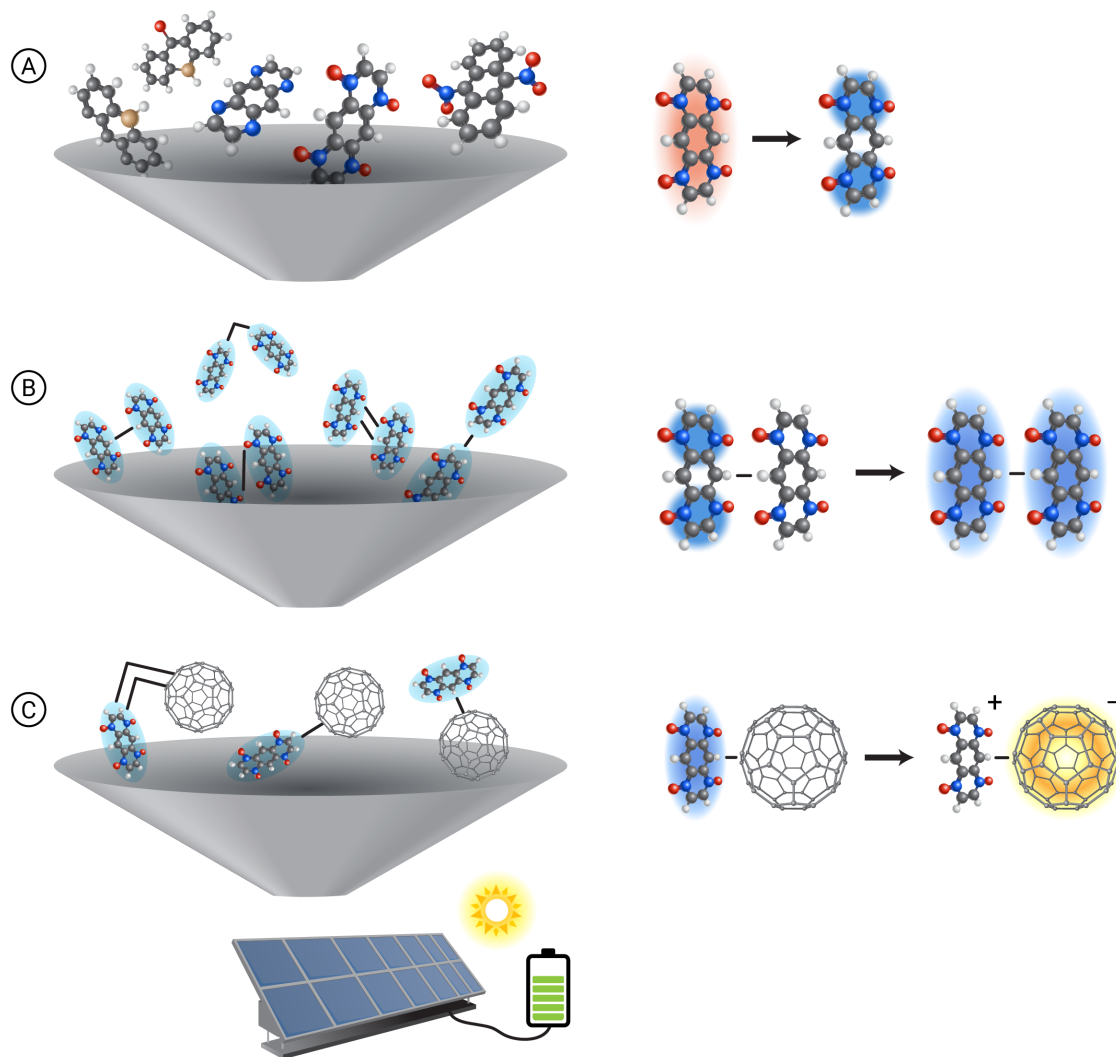


FIG. 2. A proof-of-principle SF chromophore design pipeline utilizing the iterative workflow from Fig. 1, with stages for (A) singlet fission, (B) triplet separation, and (C) charge transfer optimization. (A): A set of candidate SF chromophores is assessed based on the theoretical rate of singlet fission. Depicted is a set of anthracene derivatives generated via functional group and heteroatom substitutions (left) and a pictorial description of the SF process (right), where a singlet exciton state (red) converts to two triplets (blue) localized at the ends of the chromophore. (B): Following the selection of an SF chromophore, covalent linking strategies are optimized to enable efficient triplet separation. Various bridges and conformational arrangements would be assessed (left) to provide the most rapid triplet separation, where a triplet-pair local to a single SF chromophore converts to two triplets isolated to individual chromophores (right). (C): Finally, the charge transfer rate could be optimized using different chromophore/acceptor strategies, such as chromophore/acceptor covalent linking (left), in analogy to the optimization of step (B), to ensure efficient transfer from a triplet exciton to a charge-separated state at the acceptor interface (right).

B. Design pipeline

Achieving a high internal quantum efficiency in an SF-based photovoltaic cell depends not only on SF taking place but also on various subsequent processes prior to the generation of free-charge carriers. For one, following SF, triplets must separate so they can migrate to the chromophore-acceptor interface of the photovoltaic cell. Finally, migrated triplets must efficiently undergo a charge transfer with an acceptor at this interface to produce a pair of free charge carriers. Not only is the SF process itself non-adiabatic, but triplet separation and chromophore-acceptor charge transfer typically involve nuclear motion as well, as their portrayal involves conical intersections or avoided crossings [127–129], making their dynamics difficult to describe classically. To date, a severely limited number of works have addressed atomistic simulation of the non-adiabatic dynamics involved in triplet separation [129] and

System	# Qubits	# Toffoli Gates	Parameters
(NO) ₄ -Anth [60]	148	8.9×10^8	$N = 5, M = 19, K = 16,$ $t = 100\text{fs}, \epsilon = 10\%$
	154	2.9×10^9	$N = 5, M = 19, K = 16,$ $t = 100\text{fs}, \epsilon = 1\%$
(NO) ₄ -Anth Dimer [129]	160	1.8×10^9	$N = 6, M = 21, K = 16,$ $t = 100\text{fs}, \epsilon = 1\%$
	164	2.0×10^{10}	$N = 6, M = 21, K = 16,$ $t = 500\text{fs}, \epsilon = 1\%$
Anth/C ₆₀ [63]	117	1.5×10^7	$N = 4, M = 11, K = 16,$ $t = 100\text{fs}, \epsilon = 1\%$
	1065	2.7×10^9	$N = 4, M = 246, K = 16,$ $t = 100\text{fs}, \epsilon = 1\%$

TABLE I. Estimated implementation costs of our quantum algorithm on various systems of interest. The model on top is a $N = 5$ state $M = 19$ mode quadratic vibronic coupling (QVC) singlet fission model analyzed at 10% and 1% error tolerances, representing decision vs. quantitative problem requirements as per Section IV B 1. Next, a QVC triplet separation model with $N = 6$ states and $M = 21$ modes is analyzed for time propagations of $t = 100$ femtoseconds and $t = 500$ femtoseconds. Lastly, we analyze a $N = 4$ state linear coupling (LVC) model of charge transfer in a reduced dimensionality setting of $M = 11$ modes and the full dimensionality of $M = 246$ modes. For all entries, we discretize each mode into $K = 16$ grid points, with all estimates derived from commutator bounds in a second-order Trotter product formula. Note: commutator bounds generally overestimate the runtime, often by orders of magnitude; hence, the true runtimes are likely even more favorable.

chromophore-acceptor charge transfer [63]. This is inadequate since all three non-adiabatic processes are important in an SF-promoted photovoltaic cell. Ideally, the photon-to-exciton generation efficiency is doubled, the triplet pairs readily separate, and each triplet converts to a pair of charge carriers. In the following, we describe each of these processes in further detail and develop an SF chromophore/acceptor design pipeline illustrated in Fig. 2. We outline promising computational search spaces for each characteristic of interest to apply the quantum-enabled discovery workflow of Fig. 1 to each of the dynamical processes discussed.

1. Singlet fission

SF is the process of a photoexcited chromophore in the first excited singlet state, S_1 , transferring energy to a neighboring chromophore in its ground state S_0 , generating two *triplet* excitons:



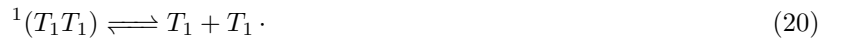
Since the pair of triplets (T_1) is coupled as an overall singlet state denoted ${}^1(T_1T_1)$, SF is a spin-allowed process. Hence, it can happen on a sub-picosecond timescale and outcompete decay pathways such as fluorescence from S_1 . One feasible approach to designing improved SF chromophores is through the derivatization of known molecular classes that undergo SF or have the potential to undergo SF [130, 131]. Derivatization involves the chemical modification of a molecule to create derivatives with altered properties, often including the introduction or modification of functional groups. For instance, a chromophore with record-breaking fast SF was proposed by introducing four N-oxyl (NO) radical fragments to anthracene [60], which we call (NO)₄-Anth. A challenge faced by the functional group modulation of SF chromophores is searching through the space of possible functional groups and their specific positionings on the parent molecule. We hope this challenge can be overcome via fast and efficient quantum dynamics simulations on a quantum computer.

Following the substitution of a functional group of a candidate molecule, a vibronic Hamiltonian that includes the relevant states must be generated to perform the corresponding dynamics. A minimal model to study the SF process consists of three states with diabats for $|S_0S_1\rangle$, $|T_1T_1\rangle$, and a charge-transfer anion-cation state $|AC\rangle$ which can facilitate the transfer. For a more complete picture, one can include complimentary $|S_1S_0\rangle$ and $|CA\rangle$ diabats, resulting in a five-state model. To simulate the SF process using our quantum algorithm, the initial state $|\psi(0)\rangle = |S_0S_1\rangle \otimes_{r=0}^{M-1} |\chi_0\rangle$ is prepared as described in Section III C. Then, time evolution is performed with the algorithm in Section III yielding $|\psi(t)\rangle = e^{iHt} |\psi(0)\rangle$, from which state populations can be extracted as in Eq.(17). By monitoring the population shift from $|S_0S_1\rangle$ to $|T_1T_1\rangle$ over time, a quantitative estimate of the SF rate is obtained. Further, state populations could offer valuable insights into the SF mechanism, e.g., the participation of $|AC\rangle/|CA\rangle$, [132] that practitioners could use to devise or reform improved rational design principles.

For screening purposes, quantum simulation could be used to study candidate SF chromophores in various ways. For instance, either to answer the decision problem “Does ultrafast SF occur?” or the more quantitative question, “What exactly is the transfer rate between the corresponding states?”. In general, answering the first question requires fewer resources since one can get away with a lower accuracy in the simulation as we only care if there has been a non-negligible population transfer to the $|T_0T_1\rangle$ state. For the second question, in contrast, we need a more accurate simulation as we care about the exact population. To illustrate the feasibility of our quantum algorithm within a discovery pipeline, we estimate the implementation cost for a realistic intramolecular SF chromophore. In particular we estimate, using commutator bounds, the cost of running our quantum algorithm for $t = 100$ femtoseconds on the $N = 5$ state, $M = 19$ mode model of $(\text{NO})_4$ -Anth from Ref. [60] for both a decision type problem at 10% error tolerance and a quantitative problem at 1% error tolerance. We find they require 148 qubits and 154 qubits as well as $\sim 8.9 \times 10^8$ and $\sim 2.9 \times 10^9$ Toffoli gates correspondingly as shown in Table I. This model has been previously studied via non-adiabatic dynamics, which predicted it to have the fastest singlet fission rate [60]. It is, hence, an excellent example of a system that may be probed throughout a molecular design workflow for SF materials.

2. Triplet separation

Following the generation of a triplet pair $^1(T_1T_1)$, the triplets might recombine or undergo other dynamical processes that lower the exciton yield. Furthermore, immobile $^1(T_1T_1)$ triplet pairs are difficult to harvest into charge carriers. A crucial step in retaining the efficiency gain offered by SF is triplet separation,



Due to the general difficulty in its assessment, the rate of triplet separation following SF is a crucial performance metric often left unexplored by current computational screening approaches. A complicating aspect is that the separation of triplets is highly sensitive to the spatial arrangement of chromophores [133, 134]. Intramolecular SF (iSF) chromophores have been a subject of dedicated interest, in which chromophores are covalently embedded in one molecular frame, allowing for the SF efficiency to be modulated systematically by tuning the covalent linker. In analogy, the triplet separation rate can be tuned by covalent linkage of chromophores. Hence, both SF and triplet separation can be made intramolecular. The concept of intramolecular triplet separation is as novel as iSF was a decade ago and has yet to be systematically explored. Herein, we describe how the general workflow of Fig. 1 could be used to optimize over covalent linkers for intramolecular triplet separation, graphically presented in Fig. 2 (B). After generating a set of candidate covalent frameworks with connected iSF chromophores, one can construct a corresponding vibronic Hamiltonian and monitor the state population transfer from an initial monomeric triplet pair, $|MTP\rangle$, to a dimeric triplet pair $|DTP\rangle$. The MTP state describes one chromophore in its triplet-pair state $^1(T_1T_1)$ and the other in its S_0 ground state. The DTP state describes the triplet-separated state, where each iSF chromophore now holds an individual triplet state across the covalent bridge. The rate of this state transfer could then be optimized by modifying the chromophore linking.

Since intramolecular triplet separation has yet to be systematically explored, the construction of an appropriate diabatic Hamiltonian has yet to be pursued. Ref. [129] performs the non-adiabatic dynamics on a vibronic Hamiltonian to describe the *intermolecular* triplet separation for a $(\text{NO})_4$ -Anth dimer system with $N = 6$ states and $M = 21$ vibrational modes. We use a modified version of this vibronic Hamiltonian as a proxy to assess the resource requirements for performing future intramolecular triplet separation simulations using our quantum algorithm. In the original setup, an additional nuclear degree of freedom R is included to describe the distance between monomers, and vibronic interactions are turned on/off using this R dependency. Within the context of intramolecular triplet separation, R would be fixed by a covalent bridge. We hence drop this degree of freedom and replace any R -dependent potentials with their values in the $R = 3.2 \text{ \AA}$ interaction region [129] to emulate the intramolecular triplet separation. In Table I, we report quantum resource estimations for the modified model of $(\text{NO})_4$ -Anth dimer triplet separation.

3. Charge transfer

Following the migration of a separated triplet exciton to the chromophore-acceptor interface, a charge transfer must occur between the excited chromophore, acting as the donor (D), and an electron acceptor (A),



generating a hole-electron pair that gathers at electrodes, transitioning to free charge carriers. To achieve an overall high internal quantum efficiency, triplet excitons residing on the SF chromophores must inject electrons efficiently

into the acceptors. Unfortunately, much like the pool of SF chromophores themselves, there is a very limited number of known viable acceptors for SF-based chromophores. Secondly, the most widely studied class of acceptors are fullerenes, which possess poor chemical stability in the presence of acene-based SF chromophores, significantly limiting their applicability [135]. There is an urgent need to discover new viable chromophore/acceptor pair systems, which could be accelerated via computational search. Electron transfer processes can occur on ultrafast timescales, involving multiple excited-state pathways along various vibrational degrees of freedom. These systems, hence, often exhibit challenging cases of non-adiabatic dynamics [63, 136, 137], and represent an entire class of industrially relevant simulation instances where our quantum algorithm could provide an advantage over classical methods.

Herein, we describe how our quantum-enabled workflow could be leveraged to design promising chromophore-acceptor interfaces. Similarly to SF and triplet separation, charge transfer is sensitive to the donor-acceptor configuration [138]. Of course, chemical reactivity also depends on the spatial arrangement of the two species. One feasible approach to tuning both these parameters is through covalent chromophore-acceptor linking. In principle, given an SF chromophore, both the choice of acceptor molecule and the chromophore-acceptor linking strategy could be optimized. Following the choice of acceptor and covalent chromophore/acceptor bridge, a vibronic Hamiltonian modelling the electron transfer process must be constructed. A minimal model of charge transfer at the chromophore/acceptor interface consists of the photogenerated chromophore excitonic state $|XT\rangle$, and the charge-separated state $|CS\rangle$ [137]. However, a more complete picture would include potentially many intermediate and charge-separated states $\{|CS_i\rangle\}_i$, and in the context of donor-bridge-acceptor systems, various intermediate bridge charge-transfer states $\{|CT_j\rangle\}_j$ [139]. To probe the charge transfer dynamics, an initial state with electronic component in the $|XT\rangle$ state would be prepared and propagated under e^{iHt} . The charge transfer process would be monitored via sampling diabatic populations $|CS_i\rangle$ at various time intervals, from which a quantitative charge transfer rate may be fitted. Observing the dynamics through monitoring electronic state populations would potentially offer valuable new information about charge transfer pathways at the chromophore-acceptor interface.

To assess the quantum resource requirements for the simulation of a realistic SF-based chromophore/acceptor electron transfer process, we utilize the anthracene/ C_{60} (Anth/ C_{60}) model described in Ref. [63]. Fullerene C_{60} is the prototypical acceptor of SF-based solar cells [140], and various anthracene-based SF chromophores have been proposed [141, 142], making Anth/ C_{60} a suitable representative for systems which may be assessed during the quantum-enabled charge transfer optimization step of Fig. 2 (C). We report the quantum resource estimation in Table I. To compare our resource estimates with classical methods, Ref. [63] required a highly optimized multi-layer MCTDH tree to perform the vibronic dynamics including $N = 4$ states and all $M = 246$ modes; furthermore, the largest standard MCTDH calculation was limited to $M = 11$ selected modes which took 155 CPU hours [63]. Furthermore, both the full and reduced models utilized a rather simplified form of vibronic Hamiltonian, where constant interstate couplings $W_{i\neq j} = \lambda^{(i,j)}$ and linear intrastate couplings $W_{ii} = \lambda^{(i,i)} + \sum_r a_r^{(i,i)} Q_r$ are used. More accurate parameterizations of the Anth/ C_{60} vibronic Hamiltonian, such as a full QVC model or beyond, quickly become prohibitive to address via state-of-the-art classical methods, whereas our quantum algorithm's runtime would still have favorable scaling. Furthermore, modeling the interface charge transfer dynamics could be made even more realistic by including more chromophore or acceptor molecules. The charge transfer dynamics at the chromophore/acceptor interface hence presents a promising future direction for utilizing a quantum computer to address impactful non-adiabatic dynamics simulations.

V. DISCUSSION

In this work, we have presented a highly optimized quantum algorithm to implement time evolution under a general vibronic Hamiltonian. Our algorithm is the first in its ability to treat an arbitrary number of electronic states and an arbitrary expansion order of the diabatic potential. Moreover, we develop various algorithmic innovations to reduce the cost of the algorithm, further making it more desirable for implementation. Next, we demonstrate that, unlike many quantum algorithms, our method is not bottlenecked by the input-output problem. Specifically, we show that not only is the cost of preparing relevant initial states negligible but also the key observable in vibronic simulation, electronic state populations, can be extracted by simply measuring a few qubits in the computational basis after time evolution. It's worth noting that we have not addressed the construction of the vibronic Hamiltonian itself (i.e., calculating the coupling parameters that define the model). This often presents its own challenges as it requires electronic structure calculations and diabaticization of the potential surfaces. There is, however, progress being made in large-scale excited-state electronic structure [3, 143, 144], automatic diabaticization protocols [24, 76], and machine learning approaches [145–149], which would assist in alleviating this bottleneck. Quantum computers could also be utilized in the electronic structure calculations.

Next, we discussed a potential application of our algorithm for industrially relevant problems by outlining a high-level pipeline for the design of singlet fission (SF) solar cells. We showed how our algorithm can be used to probe and optimize for the rates of vibronically driven energy and charge transfer processes important to the overall photovoltaic efficiency. Crucially, the pipeline covers the two important steps following SF: triplet separation and charge transfer. To date, most research in this field has been dedicated to the fission process itself, inadequately leaving the kinetics of the following processes unclear. This pipeline presents an example of where non-adiabatic quantum dynamics could lead to a paradigm shift in the field, fully enabled by the presented quantum algorithm. We note that an economically feasible integration of SF chromophores in organic photovoltaics is also limited by other factors, such as practical synthesis routes, stability under incident light, and resilience against chemical and thermal degradation [98]. While our algorithm for dynamics cannot directly assess such additional properties, it can accelerate the discovery of promising SF chromophores and extend the regrettably small pool of available candidates, which is one of the most significant barriers in the development of SF-based solar cells [58–62].

VI. ACKNOWLEDGEMENTS

The authors thank Ilya G. Ryabinkin and Michael Schuurman for stimulating discussions. We also thank Zhenggang Lan and Jiawei Peng for providing the vibronic Hamiltonian parameters for the anthracene/ C_{60} electron transfer model from Ref. [63] used in Section IV B. A.A.-G. thanks Anders G. Frøseth for his generous support, and acknowledges the generous support of Natural Resources Canada and the Canada 150 Research Chairs program. T.Z. thanks the Natural Sciences and Engineering Research Council (NSERC) of Canada (RGPIN-2024-06286) for financial support and the Digital Research Alliance of Canada for computational resources.

-
- [1] Y. Cao, J. Romero, J. P. Olson, M. Degroote, P. D. Johnson, M. Kieferová, I. D. Kivlichan, T. Menke, B. Peropadre, N. P. Sawaya, *et al.*, Quantum chemistry in the age of quantum computing, *Chem. Rev.* **119**, 10856 (2019).
 - [2] S. Lee, J. Lee, H. Zhai, Y. Tong, A. M. Dalzell, A. Kumar, P. Helms, J. Gray, Z.-H. Cui, W. Liu, M. Kastoryano, R. Babbush, J. Preskill, D. R. Reichman, E. T. Campbell, E. F. Valeev, L. Lin, and G. K.-L. Chan, Evaluating the evidence for exponential quantum advantage in ground-state quantum chemistry, *Nature Communications* **14**, 1952 (2023).
 - [3] S. Mai and L. González, Molecular photochemistry: recent developments in theory, *Angew. Chem* **59**, 16832 (2020).
 - [4] D. R. Yarkony, Nonadiabatic quantum chemistry—past, present, and future, *Chem. Rev.* **112**, 481 (2012).
 - [5] R. Long, O. V. Prezhdo, and W. Fang, Nonadiabatic charge dynamics in novel solar cell materials, *Comput. Mol. Sci.* **7**, e1305 (2017).
 - [6] T. Nelson, S. Fernandez-Alberti, A. E. Roitberg, and S. Tretiak, Nonadiabatic excited-state molecular dynamics: Modeling photophysics in organic conjugated materials, *Acc. Chem. Res.* **47**, 1155 (2014).
 - [7] C. A. Goodwin, F. Ortu, D. Reta, N. F. Chilton, and D. P. Mills, Molecular magnetic hysteresis at 60 kelvin in dysprosocenium, *Nature* **548**, 439 (2017).
 - [8] D. Reta, J. G. Kragoskow, and N. F. Chilton, Ab initio prediction of high-temperature magnetic relaxation rates in single-molecule magnets, *J. Am. Chem. Soc.* **143**, 5943 (2021).
 - [9] J. K. Staab and N. F. Chilton, Analytic linear vibronic coupling method for first-principles spin-dynamics calculations in single-molecule magnets, *J. Chem. Theory Comput.* **18**, 6588 (2022).
 - [10] T. J. Penfold, J. O. Johansson, and J. Eng, Towards understanding and controlling ultrafast dynamics in molecular photomagnets, *Coord. Chem. Rev.* **494**, 215346 (2023).
 - [11] A. Mattioni, J. K. Staab, W. J. Blackmore, D. Reta, J. Iles-Smith, A. Nazir, and N. F. Chilton, Vibronic effects on the quantum tunnelling of magnetisation in kramers single-molecule magnets, *Nat. Commun.* **15**, 485 (2024).
 - [12] A. Endo, K. Sato, K. Yoshimura, T. Kai, A. Kawada, H. Miyazaki, and C. Adachi, Efficient up-conversion of triplet excitons into a singlet state and its application for organic light emitting diodes, *Appl. Phys. Lett.* **98**, 083302 (2011).
 - [13] H. Uoyama, K. Goushi, K. Shizu, H. Nomura, and C. Adachi, Highly efficient organic light-emitting diodes from delayed fluorescence, *Nature* **492**, 234 (2012).
 - [14] T. J. Penfold and J. Gibson, The role of vibronic coupling for intersystem crossing and reverse intersystem crossing rates in TADF molecules, in *Highly Efficient OLEDs* (John Wiley & Sons, Ltd, 2018) Chap. 9, pp. 297–330.
 - [15] J. Eng and T. J. Penfold, Open questions on the photophysics of thermally activated delayed fluorescence, *Commun. Chem.* **4**, 91 (2021).
 - [16] C.-X. Li, W.-W. Guo, B.-B. Xie, and G. Cui, Photodynamics of oxybenzone sunscreen: Nonadiabatic dynamics simulations, *J. Chem. Phys.* **145** (2016).
 - [17] Z. Wu, M. Wang, Y. Guo, F. Ji, C. Wang, S. Wang, J. Zhang, Y. Wang, S. Zhang, B. Jin, *et al.*, Nonadiabatic dynamics mechanism of chalcone analogue sunscreen FPPO-HBr: excited state intramolecular proton transfer followed by conformation twisting, *J. Phys. Chem. B* **125**, 9572 (2021).

- [18] X. Zhao, Y. Wu, Y. Shi, Y. Liang, X. Feng, Y. Sun, S. Cui, X. Jin, M. Tao, H. Wang, *et al.*, Non-adiabatic dynamics mechanism in excited state of novel UV protective sunscreen in rice: Conical intersection promotes internal conversion, *J. Clust. Sci.* **32**, 967 (2021).
- [19] M. Wang, Z. Wu, F. Ji, C. Wang, and G. Zhao, Ultrafast nonadiabatic mechanism of plant sunscreens biflavonoids with two excited-state intramolecular proton transfer structures, *J. Lumin.* **246**, 118816 (2022).
- [20] L. Via and S. Magno, Photochemotherapy in the treatment of cancer, *Curr. Med. Chem.* **8**, 1405 (2001).
- [21] T. C. Zhu and J. C. Finlay, The role of photodynamic therapy (PDT) physics, *Med. Phys.* **35**, 3127 (2008).
- [22] G. Cui and W.-h. Fang, State-specific heavy-atom effect on intersystem crossing processes in 2-thiothymine: A potential photodynamic therapy photosensitizer, *J. Chem. Phys.* **138**, 044315 (2013).
- [23] F. Ponte, D. M. Scopelliti, N. Sanna, E. Sicilia, and G. Mazzone, How computations can assist the rational design of drugs for photodynamic therapy: photosensitizing activity assessment of a Ru (II)-BODIPY assembly, *Molecules* **27**, 5635 (2022).
- [24] S. P. Neville and M. S. Schuurman, Calculation of quasi-diabatic states within the DFT/MRCI(2) framework: The QD-DFT/MRCI(2) method, *J. Chem. Phys.* **160**, 234109 (2024).
- [25] V. K. Jaiswal, D. Aranda Ruiz, V. Petropoulos, P. Kabaciński, F. Montorsi, L. Uboldi, S. Ugolini, S. Mukamel, G. Cerullo, M. Garavelli, *et al.*, Sub-100-fs energy transfer in coenzyme NADH is a coherent process assisted by a charge-transfer state, *Nat. Commun.* **15**, 4900 (2024).
- [26] M. Barbatti, A. J. Aquino, J. J. Szymczak, D. Nachtigallová, P. Hobza, and H. Lischka, Relaxation mechanisms of UV-photoexcited DNA and RNA nucleobases, *Proc. Natl. Acad. Sci. U.S.A.* **107**, 21453 (2010).
- [27] P. R. Markwick and N. L. Doltsinis, Ultrafast repair of irradiated DNA: Nonadiabatic ab initio simulations of the guanine-cytosine photocycle, *J. Chem. Phys.* **126** (2007).
- [28] J. A. Green, M. Y. Jouybari, D. Aranda, R. Improta, and F. Santoro, Nonadiabatic absorption spectra and ultrafast dynamics of DNA and RNA photoexcited nucleobases, *Molecules* **26**, 1743 (2021).
- [29] W. Domcke, H. Koppel, and D. R. Yarkony, *Conical intersections: electronic structure, dynamics & spectroscopy*, Vol. 15 (World Scientific, 2004).
- [30] I. Bersuker, *The Jahn-Teller effect and vibronic interactions in modern chemistry* (Springer Science & Business Media, 2013).
- [31] H.-D. Meyer, F. Gatti, and G. A. Worth, *Multidimensional quantum dynamics: MCTDH theory and applications* (John Wiley & Sons, 2009).
- [32] J. C. Tully, Molecular dynamics with electronic transitions, *J. Chem. Phys.* **93**, 1061 (1990).
- [33] S. Chapman, The classical trajectory-surface-hopping approach to charge-transfer processes, *Adv. Chem. Phys.: State-Selected and State-To-State Ion-Molecule Reaction Dynamics, Part 2, Theory* **82**, 423 (1992).
- [34] D. L. Thompson, *Modern methods for multidimensional dynamics computations in chemistry* (World Scientific, 1998).
- [35] J. E. Subotnik, A. Jain, B. Landry, A. Petit, W. Ouyang, and N. Bellonzi, Understanding the surface hopping view of electronic transitions and decoherence, *Annu. Rev. Phys. Chem.* **67**, 387 (2016).
- [36] X. Li, J. C. Tully, H. B. Schlegel, and M. J. Frisch, Ab initio ehrenfest dynamics, *J. Chem. Phys.* **123** (2005).
- [37] G. D. Billing, The semiclassical coupled states method, *J. Chem. Phys.* **65**, 1 (1976).
- [38] G. D. Billing, On the use of Ehrenfest's theorem in molecular scattering, *Chem. Phys. Lett.* **100**, 535 (1983).
- [39] G. D. Billing, *The quantum classical theory* (Oxford University Press, USA, 2003).
- [40] H.-D. Meyer and W. H. Miller, A classical analog for electronic degrees of freedom in nonadiabatic collision processes, *J. Chem. Phys.* **70**, 3214 (1979).
- [41] H.-D. Meyer, U. Manthe, and L. S. Cederbaum, The multi-configurational time-dependent Hartree approach, *Chem. Phys. Lett.* **165**, 73 (1990).
- [42] M. H. Beck, A. Jäckle, G. A. Worth, and H.-D. Meyer, The multiconfiguration time-dependent Hartree (MCTDH) method: a highly efficient algorithm for propagating wavepackets, *Phys. Rep.* **324**, 1 (2000).
- [43] H. Wang and M. Thoss, Multilayer formulation of the multiconfiguration time-dependent Hartree theory, *J. Chem. Phys.* **119**, 1289 (2003).
- [44] H. Wang, Multilayer multiconfiguration time-dependent hartree theory, *J. Phys. Chem. A* **119**, 7951 (2015).
- [45] I. Burghardt, K. Giri, and G. Worth, Multimode quantum dynamics using Gaussian wavepackets: The Gaussian-based multiconfiguration time-dependent Hartree (G-MCTDH) method applied to the absorption spectrum of pyrazine, *J. Chem. Phys.* **129** (2008).
- [46] G. W. Richings, I. Polyak, K. E. Spinlove, G. A. Worth, I. Burghardt, and B. Lasorne, Quantum dynamics simulations using Gaussian wavepackets: the vMCG method, *Int. Rev. Phys. Chem.* **34**, 269 (2015).
- [47] P. Marquetand, J. J. Nogueira, S. Mai, F. Plasser, and L. González, Challenges in simulating light-induced processes in DNA, *Molecules* **22**, 49 (2016).
- [48] S. Mukherjee, M. Pinheiro Jr, B. Demoulin, and M. Barbatti, Simulations of molecular photodynamics in long timescales, *Philos. Trans. R. Soc. A* **380**, 20200382 (2022).
- [49] P. J. Ollitrault, A. Miessen, and I. Tavernelli, Molecular quantum dynamics: A quantum computing perspective, *Acc. Chem. Res.* **54**, 4229 (2021).
- [50] P. Schleich, L. B. Kristensen, J. A. Angulo, D. Avagliano, M. Bagherimehrab, A. Aldossary, C. Gorgulla, J. Fitzsimons, and A. Aspuru-Guzik, Chemically motivated simulation problems are efficiently solvable by a quantum computer, arXiv preprint arXiv:2401.09268 (2024).

- [51] A. Miessen, P. J. Ollitrault, F. Tacchino, and I. Tavernelli, Quantum algorithms for quantum dynamics, *Nat. Comput. Sci.* **3**, 25 (2023).
- [52] R. J. MacDonell, C. E. Dickerson, C. J. Birch, A. Kumar, C. L. Edmunds, M. J. Biercuk, C. Hempel, and I. Kassal, Analog quantum simulation of chemical dynamics, *Chem. Sci.* **12**, 9794 (2021).
- [53] M. Kang, H. Nuomin, S. N. Chowdhury, J. L. Yuly, K. Sun, J. Whitlow, J. Valdiviezo, Z. Zhang, P. Zhang, D. N. Beratan, and K. R. Brown, Seeking a quantum advantage with trapped-ion quantum simulations of condensed-phase chemical dynamics, *Nat. Rev. Chem.* **8**, 340 (2024).
- [54] P. J. Ollitrault, G. Mazzola, and I. Tavernelli, Nonadiabatic molecular quantum dynamics with quantum computers, *Phys. Rev. Lett.* **125**, 260511 (2020).
- [55] M. B. Smith and J. Michl, Singlet fission, *Chem. Rev.* **110**, 6891 (2010).
- [56] M. B. Smith and J. Michl, Recent advances in singlet fission, *Annu. Rev. Phys. Chem.* **64**, 361 (2013).
- [57] J. Michl, Unconventional solar energy: singlet fission, *Mol. Front. J.* **3**, 84 (2019).
- [58] D. Casanova, Theoretical modeling of singlet fission, *Chem. Rev.* **118**, 7164 (2018).
- [59] D. Padula, Ö. H. Omar, T. Nematiharam, and A. Troisi, Singlet fission molecules among known compounds: finding a few needles in a haystack, *Energy Environ. Sci.* **12**, 2412 (2019).
- [60] E. Pradhan and T. Zeng, Design of the smallest intramolecular singlet fission chromophore with the fastest singlet fission, *J. Phys. Chem. Lett.* **13**, 11076 (2022).
- [61] X. Liu, X. Wang, S. Gao, V. Chang, R. Tom, M. Yu, L. M. Ghiringhelli, and N. Marom, Finding predictive models for singlet fission by machine learning, *npj Comput. Mater.* **8**, 70 (2022).
- [62] T. Zeng, N. Ananth, and R. Hoffmann, Seeking small molecules for singlet fission: a heteroatom substitution strategy, *J. Am. Chem. Soc.* **136**, 12638 (2014).
- [63] Y. Xie, J. Zheng, and Z. Lan, Full-dimensional multilayer multiconfigurational time-dependent hartree study of electron transfer dynamics in the anthracene/c60 complex, *J. Chem. Phys.* **142** (2015).
- [64] H. Köppel, W. Domcke, and L. S. Cederbaum, Multimode molecular dynamics beyond the Born-Oppenheimer approximation, in *Advances in Chemical Physics* (John Wiley & Sons, Ltd, 1984) pp. 59–246.
- [65] J. Eng, C. Gourlaouen, E. Gindensperger, and C. Daniel, Spin-vibronic quantum dynamics for ultrafast excited-state processes, *Acc. Chem. Res.* **48**, 809 (2015).
- [66] T. Zeng, A diabaticization protocol that includes spin-orbit coupling, *J. Chem. Phys.* **146** (2017).
- [67] E. Pradhan and T. Zeng, The unified Hamiltonian formalism of spin-orbit Jahn-Teller and pseudo-Jahn-Teller problems in all axial symmetries, *J. Chem. Theory Comput.* **19**, 7776 (2023).
- [68] H. Köppel, W. Domcke, and L. Cederbaum, Theory of vibronic coupling in linear molecules, *J. Chem. Phys.* **74**, 2945 (1981).
- [69] M. Nooijen, First-principles simulation of the UV absorption spectrum of ketene, *Int. J. Quantum Chem.* **95**, 768 (2003).
- [70] S. Mahapatra, W. Eisfeld, and H. Köppel, Effects of multimode Jahn-Teller coupling on the photodetachment spectrum of nitrate anion (NO_3^-), *Chem. Phys. Lett.* **441**, 7 (2007).
- [71] S. Faraji, H. Köppel, W. Eisfeld, and S. Mahapatra, Towards a higher-order description of Jahn-Teller coupling effects in molecular spectroscopy: The \tilde{A}^2E'' state of NO_3 , *Chem. Phys.* **347**, 110 (2008).
- [72] D. Aranda and F. Santoro, Vibronic spectra of π -conjugated systems with a multitude of coupled states: A protocol based on linear vibronic coupling models and quantum dynamics tested on hexahelicene, *J. Chem. Theory Comput.* **17**, 1691 (2021).
- [73] J. F. Stanton, On the vibronic level structure in the NO_3 radical. I. The ground electronic state, *J. Chem. Phys.* **126** (2007).
- [74] G. J. Atchity and K. Ruedenberg, Determination of diabatic states through enforcement of configurational uniformity, *Theor. Chem. Acc.* **97**, 47 (1997).
- [75] K. Ruedenberg and G. J. Atchity, A quantum chemical determination of diabatic states, *J. Chem. Phys.* **99**, 3799 (1993).
- [76] Y. Zhang, P. Su, B. Lasorne, B. Bräida, and W. Wu, A novel valence-bond-based automatic diabaticization method by compression, *J. Phys. Chem. Lett.* **11**, 5295 (2020).
- [77] I. Bersuker, *The Jahn-Teller Effect* (Cambridge University Press, 2006).
- [78] R. A. Lang, A. Japahuge, and T. Zeng, General formalism of vibronic hamiltonians for tetrahedral and octahedral systems: Problems that involve A-type states and a-type vibrations, *Chem. Phys.* **515**, 36 (2018).
- [79] A. Viel and W. Eisfeld, Effects of higher order Jahn-Teller coupling on the nuclear dynamics, *J. Chem. Phys.* **120**, 4603 (2004).
- [80] W. Eisfeld and A. Viel, Higher order $(A + E) \otimes e$ pseudo-Jahn-Teller coupling, *J. Chem. Phys.* **122** (2005).
- [81] S. Bhattacharyya, D. Opalka, L. V. Poluyanov, and W. Domcke, The $(E + A) \times (e + a)$ Jahn-Teller and pseudo-Jahn-Teller Hamiltonian including spin-orbit coupling for trigonal systems, *J. Phys. Chem. A* **118**, 11962 (2014).
- [82] W. Eisfeld, O. Vieuxmaire, and A. Viel, Full-dimensional diabatic potential energy surfaces including dissociation: The $^2E''$ state of NO_3 , *J. Chem. Phys.* **140** (2014).
- [83] T. Mondal, On the higher-order $T_2 \otimes (e + t_2)$ Jahn-Teller coupling effects in the photodetachment spectrum of the alanate anion (AlH_4^-), *Phys. Chem. Chem. Phys.* **20**, 9401 (2018).
- [84] M. A. Parkes and G. A. Worth, The “simple” photochemistry of thiophene, arXiv preprint arXiv:2407.20039 (2024).
- [85] J. Brown, R. A. Lang, and T. Zeng, Unified Hamiltonian formalism of Jahn-Teller and pseudo-Jahn-Teller problems in axial symmetries, *J. Chem. Theory Comput.* **17**, 4392 (2021).

- [86] A. Macridin, P. Spentzouris, J. Amundson, and R. Harnik, Digital quantum computation of fermion-boson interacting systems, *Phys. Rev. A* **98**, 042312 (2018).
- [87] A. Kitaev and W. A. Webb, Wavefunction preparation and resampling using a quantum computer, arXiv preprint arXiv:0801.0342 (2008).
- [88] L. Grover and T. Rudolph, Creating superpositions that correspond to efficiently integrable probability distributions, arXiv preprint quant-ph/0208112 (2002).
- [89] J. Iaconis, S. Johri, and E. Y. Zhu, Quantum state preparation of normal distributions using matrix product states, *npj Quantum Inf.* **10**, 15 (2024).
- [90] D. Gosset, R. Kothari, and K. Wu, Quantum state preparation with optimal t-count (2024), arXiv:2411.04790 [quant-ph].
- [91] Y. R. Sanders, G. H. Low, A. Scherer, and D. W. Berry, Black-box quantum state preparation without arithmetic, *Physical review letters* **122**, 020502 (2019).
- [92] S. Wang, Z. Wang, G. Cui, S. Shi, R. Shang, L. Fan, W. Li, Z. Wei, and Y. Gu, Fast black-box quantum state preparation based on linear combination of unitaries, *Quantum Information Processing* **20**, 270 (2021).
- [93] G. Brassard, P. Høyer, M. Mosca, and A. Tapp, Quantum amplitude amplification and estimation, *Quantum Comput. Info.* **305**, 53–74 (2002).
- [94] I. Loaiza, D. Motlagh, K. Hejazi, M. S. Zini, A. Delgado, and J. M. Arrazola, Nonlinear spectroscopy via generalized quantum phase estimation, arXiv preprint arXiv:2405.13885 (2024).
- [95] T. Kharazi, T. F. Stetina, L. Ko, G. H. Low, and K. B. Whaley, An efficient quantum algorithm for generation of ab initio n-th order susceptibilities for non-linear spectroscopies, arXiv preprint arXiv:2404.01454 (2024).
- [96] T. J. Dougherty, C. J. Gomer, B. W. Henderson, G. Jori, D. Kessel, M. Korbelik, J. Moan, and Q. Peng, Photodynamic therapy, *J. Natl. Cancer Inst.* **90**, 889 (1998).
- [97] W. Shockley and H. J. Queisser, Detailed balance limit of efficiency of p-n junction solar cells, *J. Appl. Phys.* **32**, 510 (1961).
- [98] A. J. Baldacchino, M. I. Collins, M. P. Nielsen, T. W. Schmidt, D. R. McCamey, and M. J. Y. Tayebjee, Singlet fission photovoltaics: Progress and promising pathways, *Chem. Phys. Rev.* **3**, 021304 (2022).
- [99] M. B. Smith and J. Michl, Singlet fission, *Chem. Rev.* **110**, 6891 (2010).
- [100] A. Japahuge and T. Zeng, Theoretical studies of singlet fission: Searching for materials and exploring mechanisms, *ChemPlusChem* **83**, 146 (2018).
- [101] K. M. Felter and F. C. Grozema, Singlet fission in crystalline organic materials: Recent insights and future directions, *J. Phys. Chem. Lett.* **10**, 7208 (2019).
- [102] F. Weber and H. Mori, Machine-learning assisted design principle search for singlet fission: an example study of cibalackrot, *npj Comput. Mater.* **8**, 176 (2022).
- [103] K. A. Veilleux, G. Schreckenbach, and D. E. Herbert, Designing biphenanthridine-based singlet fission materials using computational chemistry, *Mol. Syst. Des. Eng.* **9**, 423 (2024).
- [104] X. Wang, S. Gao, Y. Luo, X. Liu, R. Tom, K. Zhao, V. Chang, and N. Marom, Computational discovery of intermolecular singlet fission materials using many-body perturbation theory, *J. Phys. Chem. C* **128**, 7841 (2024).
- [105] X. Xie, Y. Liu, Y. Yao, U. Schollwöck, C. Liu, and H. Ma, Time-dependent density matrix renormalization group quantum dynamics for realistic chemical systems, *J. Chem. Phys.* **151**, 224101 (2019).
- [106] R. Tempelaar and D. R. Reichman, Vibronic exciton theory of singlet fission. I. Linear absorption and the anatomy of the correlated triplet pair state, *J. Chem. Phys.* **146** (2017).
- [107] P. E. Teichen and J. D. Eaves, A microscopic model of singlet fission, *J. Phys. Chem. B* **116**, 11473 (2012).
- [108] T. C. Berkelbach, M. S. Hybertsen, and D. R. Reichman, Microscopic theory of singlet exciton fission. I. General formulation, *J. Chem. Phys.* **138**, 114102 (2013).
- [109] T. C. Berkelbach, M. S. Hybertsen, and D. R. Reichman, Microscopic theory of singlet exciton fission. ii. application to pentacene dimers and the role of superexchange, *J. Chem. Phys.* **138** (2013).
- [110] A. A. Bakulin, S. E. Morgan, T. B. Kehoe, M. W. Wilson, A. W. Chin, D. Zigmantas, D. Egorova, and A. Rao, Real-time observation of multiexcitonic states in ultrafast singlet fission using coherent 2d electronic spectroscopy, *Nat. Chem.* **8**, 16 (2016).
- [111] H. Tamura, M. Huix-Rotllant, I. Burghardt, Y. Olivier, and D. Beljonne, First-principles quantum dynamics of singlet fission: coherent versus thermally activated mechanisms governed by molecular π stacking, *Phys. Rev. Lett.* **115**, 107401 (2015).
- [112] Y. Yao, Coherent dynamics of singlet fission controlled by nonlocal electron-phonon coupling, *Phys. Rev. B* **93**, 115426 (2016).
- [113] Y. Fujihashi, L. Chen, A. Ishizaki, J. Wang, and Y. Zhao, Effect of high-frequency modes on singlet fission dynamics, *J. Chem. Phys.* **146** (2017).
- [114] A. F. Morrison and J. M. Herbert, Evidence for singlet fission driven by vibronic coherence in crystalline tetracene, *J. Phys. Chem. Lett.* **8**, 1442 (2017).
- [115] K. Miyata, Y. Kurashige, K. Watanabe, T. Sugimoto, S. Takahashi, S. Tanaka, J. Takeya, T. Yanai, and Y. Matsumoto, Coherent singlet fission activated by symmetry breaking, *Nat. Chem.* **9**, 983 (2017).
- [116] R. Casillas, I. Papadopoulos, T. Ullrich, D. Thiel, A. Kunzmann, and D. M. Guldi, Molecular insights and concepts to engineer singlet fission energy conversion devices, *Energy Environ. Sci.* **13**, 2741 (2020).
- [117] W.-L. Chan, T. C. Berkelbach, M. R. Provorse, N. R. Monahan, J. R. Tritsch, M. S. Hybertsen, D. R. Reichman, J. Gao, and X.-Y. Zhu, The quantum coherent mechanism for singlet fission: Experiment and theory, *Acc. Chem. Res.* **46**, 1321

- (2013).
- [118] K. R. Parenti, R. Chesler, G. He, P. Bhattacharyya, B. Xiao, H. Huang, D. Malinowski, J. Zhang, X. Yin, A. Shukla, *et al.*, Quantum interference effects elucidate triplet-pair formation dynamics in intramolecular singlet-fission molecules, *Nat. Chem.* **15**, 339 (2023).
- [119] Y. Chen, L. Shen, and X. Li, Effects of heteroatoms of tetracene and pentacene derivatives on their stability and singlet fission, *J. Phys. Chem. A* **118**, 5700 (2014).
- [120] K. Bhattacharyya, S. M. Pratik, and A. Datta, Small organic molecules for efficient singlet fission: role of silicon substitution, *J. Phys. Chem. C* **119**, 25696 (2015).
- [121] J. M. Hernández-Lobato, J. Requeima, E. O. Pyzer-Knapp, and A. Aspuru-Guzik, Parallel and distributed Thompson sampling for large-scale accelerated exploration of chemical space, in *International conference on machine learning* (PMLR, 2017) pp. 1470–1479.
- [122] E. O. Pyzer-Knapp, Bayesian optimization for accelerated drug discovery, *IBM J. Res. Dev.* **62**, 2 (2018).
- [123] R.-R. Griffiths and J. M. Hernández-Lobato, Constrained bayesian optimization for automatic chemical design using variational autoencoders, *Chem. Sci* **11**, 577 (2020).
- [124] S. Ito, T. Nagami, and M. Nakano, Molecular design for efficient singlet fission, *J. Photoch. Photobio. C* **34**, 85 (2018).
- [125] T. Hasobe, S. Nakamura, N. V. Tkachenko, and Y. Kobori, Molecular design strategy for high-yield and long-lived individual doubled triplet excitons through intramolecular singlet fission, *ACS Energy Lett.* **7**, 390 (2021).
- [126] L. Wang, X. Shi, S. Feng, W. Liang, H. Fu, and J. Yao, Molecular design strategy for practical singlet fission materials: the charm of donor/acceptor decorated quinoidal structure, *CCS Chem.* **4**, 2748 (2021).
- [127] O. V. Prezhdo, W. R. Duncan, and V. V. Prezhdo, Photoinduced electron dynamics at the chromophore–semiconductor interface: A time-domain ab initio perspective, *Prog. Surf. Sci.* **84**, 30 (2009).
- [128] C. Sissa, F. Delchiaro, F. Di Maiolo, F. Terenziani, and A. Painelli, Vibrational coherences in charge-transfer dyes: A non-adiabatic picture, *J. Chem. Phys.* **141** (2014).
- [129] E. Pradhan and T. Zeng, Triplet separation after the fastest intramolecular singlet fission in the smallest chromophore, *J. Chem. Theory Comput.* **19**, 2092 (2023).
- [130] M. Zhang, Z.-M. Su, Y.-G. Li, and H.-L. Xu, Novel singlet fission chromophores: Boron/nitrogen para-substituted acenes, *Dyes Pigm.* **231**, 112414 (2024).
- [131] R. Patra and M. Das, Designing an efficient singlet fission material with b- n substitution in pyrene: A model exact study, *J. Phys. Chem. A* **128**, 7375 (2024).
- [132] S. Lukman, K. Chen, J. M. Hodgkiss, D. H. Turban, N. D. Hine, S. Dong, J. Wu, N. C. Greenham, and A. J. Musser, Tuning the role of charge-transfer states in intramolecular singlet exciton fission through side-group engineering, *Nat. Commun.* **7**, 13622 (2016).
- [133] J. C. Johnson, A. J. Nozik, and J. Michl, The role of chromophore coupling in singlet fission, *Acc. Chem. Res.* **46**, 1290 (2013).
- [134] R. J. Hudson, A. N. Stuart, D. M. Huang, and T. W. Kee, What next for singlet fission in photovoltaics? The fate of triplet and triplet-pair excitons, *J. Phys. Chem. C* **126**, 5369 (2022).
- [135] J. Xia, S. N. Sanders, W. Cheng, J. Z. Low, J. Liu, L. M. Campos, and T. Sun, Singlet fission: Progress and prospects in solar cells, *Adv. Mater.* **29**, 1601652 (2017).
- [136] A. V. Akimov and O. V. Prezhdo, Nonadiabatic dynamics of charge transfer and singlet fission at the pentacene/c60 interface, *J. Am. Chem. Soc.* **136**, 1599 (2014).
- [137] F. Di Maiolo, G. A. Worth, and I. Burghardt, Multi-layer gaussian-based multi-configuration time-dependent hartree (ml-gmctdh) simulations of ultrafast charge separation in a donor–acceptor complex, *J. Chem. Phys.* **154** (2021).
- [138] B.-C. Lin, B. T. Koo, P. Clancy, and C.-P. Hsu, Theoretical investigation of charge-transfer processes at pentacene–C60 interface: the importance of triplet charge separation and Marcus electron transfer theory, *J. Phys. Chem. C* **118**, 23605 (2014).
- [139] S. Mandal and C. Daniel, Ultrafast excited-state nonadiabatic dynamics in pt (ii) donor–bridge–acceptor assemblies: A quantum approach for optical control, *J. Phys. Chem. A* **128**, 3126 (2024).
- [140] D. N. Congreve, J. Lee, N. J. Thompson, E. Hontz, S. R. Yost, P. D. Reusswig, M. E. Bahlke, S. Reineke, T. Van Voorhis, and M. A. Baldo, External quantum efficiency above 100% in a singlet-exciton-fission–based organic photovoltaic cell, *Science* **340**, 334 (2013).
- [141] J. K. H. Pun, J. K. Gallaher, L. Frazer, S. K. Prasad, C. B. Dover, R. W. MacQueen, and T. W. Schmidt, Tips-anthracene: a singlet fission or triplet fusion material?, *J. Photonics Energy* **8**, 022006 (2018).
- [142] E. Pradhan, S. Lee, C. H. Choi, and T. Zeng, Diboron-and diaza-doped anthracenes and phenanthrenes: their electronic structures for being singlet fission chromophores, *J. Phys. Chem. A* **124**, 8159 (2020).
- [143] J. W. Snyder Jr, B. F. Curchod, and T. J. Martínez, GPU-accelerated state-averaged complete active space self-consistent field interfaced with ab initio multiple spawning unravels the photodynamics of provitamin D3, *J. Phys. Chem. Lett.* **7**, 2444 (2016).
- [144] D. Hollas, L. Sistik, E. G. Hohenstein, T. J. Martinez, and P. Slavicek, Nonadiabatic ab initio molecular dynamics with the floating occupation molecular orbital-complete active space configuration interaction method, *J. Chem. Theory Comput.* **14**, 339 (2018).
- [145] W.-K. Chen, X.-Y. Liu, W.-H. Fang, P. O. Dral, and G. Cui, Deep learning for nonadiabatic excited-state dynamics, *J. Phys. Chem. Lett.* **9**, 6702 (2018).

- [146] W.-K. Chen, W.-H. Fang, and G. Cui, Integrating machine learning with the multilayer energy-based fragment method for excited states of large systems, *J. Phys. Chem. Lett.* **10**, 7836 (2019).
- [147] H. Kawai and Y. O. Nakagawa, Predicting excited states from ground state wavefunction by supervised quantum machine learning, *Mach. Learn.: Sci. Technol.* **1**, 045027 (2020).
- [148] J. Westermayr and P. Marquetand, Machine learning for electronically excited states of molecules, *Chem. Rev.* **121**, 9873 (2021).
- [149] F. Ghalami, P. M. Dohmen, M. Krämer, M. Elstner, and W. Xie, Nonadiabatic simulation of exciton dynamics in organic semiconductors using neural network-based Frenkel Hamiltonian and gradients, *J. Chem. Theory Comput.* **20**, 6160 (2024).
- [150] Y. Su, D. W. Berry, N. Wiebe, N. Rubin, and R. Babbush, Fault-tolerant quantum simulations of chemistry in first quantization, *PRX Quantum* **2**, 040332 (2021).
- [151] C. Gidney, Halving the cost of quantum addition, *Quantum* **2**, 74 (2018).

Appendix A: Complexity Analysis

Here we provide a proof for Theorem 1

Theorem 1. *Let N be the number of electronic states, M be the number of vibrational modes, and K be the number of grid points per mode. Define the vibronic Hamiltonian as $H = \mathbb{I}_{el} \otimes \sum_{r=0}^{M-1} \frac{\omega_r}{2} P_r^2 + \sum_{j,i=0}^{N-1} |j\rangle \langle i| \otimes V_{ji}$, where each $V_{ji} = \sum_{|\vec{\alpha}| \leq d} c_{\vec{\alpha}}^{(j,i)} \mathbf{Q}^{\vec{\alpha}}$ is a d -degree multivariate polynomial of position operators. Let H_m be defined as in Eq. (7) for $0 \leq m < N$ and let $H_N = \mathbb{I}_{el} \otimes \sum_{r=0}^{M-1} \frac{\omega_r}{2} P_r^2$ so $H = \sum_{m=0}^N H_m$. Then for $\epsilon, \theta \in [0, 1]$ we can implement*

$$\prod_{m=0}^N e^{i\theta H_m + \mathcal{O}(\epsilon)},$$

using $\mathcal{O}(NM^d [d \log(K)^2 + \log(M^d/\epsilon)] + N^2 \log(N))$ T gates and $\mathcal{O}(d^2 \log(MK) + d \log(1/\epsilon) + N)$ ancilla qubits.

Proof of Theorem 1. Let $N \in \mathbb{N}^+$ be the number of electronic states, $M \in \mathbb{N}_{>1}$ be the number of vibrational modes, $K \in \mathbb{N}^+$ be the number of grid points per mode, $d \in \mathbb{N}^+$ be the expansion order of the potential, $\epsilon \in [0, 1]$ be the precision parameter, and let $\theta \in [0, 1]$ be the time step. For the following, we assume the polynomial coefficients are given as floating-point numbers of constant lengths. Note that the cost of a single first-order Trotter step

$$\prod_{m=0}^N e^{i\theta H_m + \mathcal{O}(\epsilon)}, \tag{A1}$$

reduces to that of implementing the exponentials of all fragments H_m up to accuracy ϵ . First, notice that since

$$P = \text{QFT}^\dagger \cdot (X_{k-1} \otimes I) Q (X_{k-1} \otimes I) \cdot \text{QFT}, \tag{A2}$$

the cost of implementing $e^{i\theta H_N + \mathcal{O}(\epsilon)}$ will be $2M$ times the cost of $\log(K)$ -qubit QFTs, M squaring of $\log(K)$ -qubit registers, $2M$ multiplications/unmultiplication of $2 \log(K)$ -qubit registers with floating-point numbers of constant lengths and M phase gradient operations of accuracy ϵ/M for a total non-Clifford cost of $\mathcal{O}(M [\log(K)^2 + \log(M/\epsilon)])$. Hence, for the rest of the proof, we'll focus on the cost of implementing $e^{i\theta H_m + \mathcal{O}(\epsilon)}$ for $0 \leq m < N$.

In Section III, we show how to block-diagonalize each fragment H_m using only Clifford gates, after which the exponential of the corresponding H_m can be implemented in the same manner as the exponential of H_0 . Therefore, the total cost of implementing Eq. (A1) is N times that of $e^{i\theta H_0 + \mathcal{O}(\epsilon)}$. Hence it suffices to show $e^{i\theta H_0 + \mathcal{O}(\epsilon)}$ can be implemented with non-Clifford cost of $\mathcal{O}(M^d [d \log(K)^2 + \log(M^d/\epsilon)] + N \log(N))$ using $\mathcal{O}(d^2 \log(MK) + d \log(1/\epsilon) + N)$ ancilla qubits.

Notice that $e^{i\theta H_0} = e^{i\theta \sum_j |j\rangle \langle j| \otimes V_{jj}} = \sum_j |j\rangle \langle j| \otimes e^{i\theta V_{jj}}$ is a sequence of evolutions, $e^{i\theta V_{jj}}$, on the vibrational space controlled by the corresponding state $|j\rangle$ in the electronic register. In Section III we show that the cost of the multiplexed time evolution $\sum_j |j\rangle \langle j| \otimes e^{i\theta V_{jj}}$ reduces to the cost of the multiplexing of the coefficients being loaded plus the cost of an uncontrolled exponential of a single $e^{i\theta V_{jj}}$ on the vibrational space. Notice that loading coefficients controlled on a single qubit can be done using only Clifford gates (CNOTs), and a multi-control loading can be done by applying a multi-controlled X gate on a clean ancilla and then using that ancilla to perform a singly controlled loading of the coefficient followed by another multi-controlled X gate on the ancilla to put it back into a clean state.

Then, for our multiplexed loading of the coefficients, we use N clean ancilla qubits, each representing one state $|j\rangle$ of the electronic register. We then apply an X gate on each of them, controlled by the corresponding state of the electronic register they represent. Then, each ancilla can be used to load the corresponding state's coefficients. After implementing all corresponding monomials, we put the ancilla's back into their clean state again by applying an X gate on them, controlled by the corresponding state of the electronic register they represented. Since there are N electronic states, each resulting in $2 \log(N)$ -controlled X gates, the multiplexed loading of the coefficients can be done with a non-Clifford cost $\mathcal{O}(N \log N)$ and $\mathcal{O}(N)$ ancillas. Then all that remains to show is that a single $e^{i\theta V_{jj}}$ can be implemented with non-Clifford cost of $\mathcal{O}(M^d [d \log(K)^2 + \log(M^d/\epsilon)])$ using $\mathcal{O}(d^2 \log(MK) + d \log(1/\epsilon))$ ancilla qubits.

Given the caching algorithm in Section III A, implementation of each monomial of degree $s > 1$ in V_{jk} reuses the computation from a degree $s - 1$ monomial and multiplies the degree $s - 1$ variable with a degree 1 variable to get the s degree variable. Hence, the cost of computing an s -degree variable is [150]

$$2(s - 1) \log(K)^2 - (s - 1) \log(K) \sim \mathcal{O}(s \log(K)^2), \quad (\text{A3})$$

and assuming a fixed-point representation of the corresponding coefficient of the monomial, the cost of multiplying the $s \log(K)$ bit variable with its corresponding coefficient is $\sim \mathcal{O}(s \log(K))$. Lastly, we perform the b-qubit phase gradient operation with scaling factor $(\sqrt{2\pi/K})^s$ via quantum addition to a b-qubit resource register as described in [151]. This has cost $\sim \mathcal{O}(b)$ Toffolis. Since we need to set $b \sim \mathcal{O}(\log(M^d/\epsilon))$ to meet the required accuracy, then the total cost of exponentiating each monomial of degree s in V_{jj} is $\sim \mathcal{O}(s \log(K)^2 + \log(M^d/\epsilon))$. Since there are M^s monomials of degree s for $1 \leq s \leq d$, exponentiating V_{jj} has cost

$$\mathcal{O}\left(\sum_{s=1}^d M^s (s \log(K)^2 + \log(M^d/\epsilon))\right) \sim \mathcal{O}(M^d (d \log(K)^2 + \log(M^d/\epsilon))) \quad (\text{A4})$$

Lastly, as mentioned above, we need an ancillary $\log(M^d/\epsilon)$ -qubit register per degree $1 \leq s \leq d$ to perform our phase gradient operations. We also need an ancillary $s \log(K)$ register to cache a variable of degree s for all $1 < s < d$. This adds up to $\mathcal{O}(d^2 \log(K) + d \log(M^d/\epsilon)) = \mathcal{O}(d^2 \log(MK) + d \log(1/\epsilon))$ ancilla qubits. \square